DOI: 10.37190/abb/221631

Application of Magnetic Hyperthermia in Prostate Cancer Treatment

Dorota Szymańska[1], Łukasz Fuśnik[2], Arkadiusz Miaskowski[1*]

[1]Lublin University of Technology, Department of Electronics and Information Technologies, Lublin, Poland

[2]AGH, University of Science and Technology, Institute of Electronics, Krakow, Poland

*Corresponding author: Arkadiusz Miaskowski, Lublin University of Technology, Department of Electronics and Information Technologies, Lublin, Poland, e-mail address: a.miaskowski@pollub.pl

Submitted: 11th April 2026

Accepted: 8th May 2026

Abstract

Purpose

The aim of this study was to determine the required concentration of magnetic nanoparticles to achieve the therapeutic temperature in prostate cancer treatment during magnetic hyperthermia, taking into account the influence of the geometry of the heated region. In this context four types of magnetic nanoparticles were considered in the calculations: maghemite, magnetite, cobalt ferrite and barium ferrite.

Methods

An air coil generating an alternating magnetic field was designed to obtain a uniform magnetic field distribution in the prostate region. The magnetic field distribution was used to calculate the volumetric power density generated by the magnetic nanoparticles. Thermal simulations were conducted for a naturalistic prostate tumour and three geometric primitives (cylinder, sphere and cube) placed in the same anatomical location for comparison purposes. To evaluate the concentration of various types of magnetic nanoparticles, the Linear Response Theory was used.

Results

The concentrations of magnetic nanoparticles for the tumour, cylinder, sphere and cube required to achieve the therapeutic temperature were determined. The results revealed noticeable differences between the tumour model and simplified geometries in terms of both required nanoparticle concentration and heating efficiency.

Conclusions

The obtained results indicate that the concentration of magnetic nanoparticles required to achieve therapeutic temperatures strongly depends on the geometry of the heated region, type of magnetic nanoparticles and their concentration. Furthermore, the use of simplified geometrical models may lead to significant inaccuracies in predicting heat generation, suggesting that realistic tumour geometry should be considered in magnetic hyperthermia studies. These findings highlight the necessity of individualized treatment planning.

Keywords: hyperthermia, magnetic nanoparticles, prostate cancer, computer simulation.

1. Introduction

Prostate cancer is the second most commonly diagnosed cancer among men worldwide and one of the leading causes of cancer-related mortality in the male population. Its treatment poses a serious challenge [16]. Conventional therapeutic approaches include prostatectomy, radiotherapy, hormone therapy and chemotherapy. Although these treatments are widely used in clinical practice, they are often associated with substantial side effects and do not always provide satisfactory therapeutic outcomes, particularly in advanced stages of the disease. Consequently, the development of new therapeutic strategies that are both effective and minimally invasive remains an important research objective [18][20].

One of the promising therapeutic approaches currently investigated is hyperthermia therapy, which involves controlled heating of tumour tissue to temperatures typically ranging from 42 °C to 45 °C. At these temperatures, cancer cells become more susceptible to thermal damage and apoptosis, while normal tissues can tolerate such thermal exposure for limited periods of time. Furthermore, hyperthermia has been shown to significantly enhance the effectiveness of other therapeutic modalities such as radiotherapy and chemotherapy by improving tumour perfusion and oxygenation and by increasing the sensitivity of cancer cells to radiation and cytotoxic drugs [23].

Among the different hyperthermia techniques, magnetic hyperthermia has attracted considerable attention due to its ability to generate localized heating within tumour tissue using magnetic nanoparticles exposed to an alternating magnetic field. In this method, magnetic nanoparticles are introduced into the tumour region and subsequently subjected to an external alternating magnetic field, which leads to the dissipation of electromagnetic energy in the form of heat [10]. This approach enables relatively precise control of heat generation within the targeted region and therefore may significantly reduce damage to surrounding healthy tissues.

The mechanism of heat generation in magnetic nanoparticles is mainly related to magnetic relaxation processes occurring within the particles. Two primary mechanisms are responsible for this phenomenon: Néel relaxation and Brownian relaxation. Néel relaxation involves the reorientation of the magnetic moment inside the nanoparticle without physical rotation of the particle itself, whereas Brownian relaxation is associated with the rotational motion of the entire nanoparticle in a viscous medium [19][22]. The effective relaxation time of the nanoparticles is determined by the combined contribution of these mechanisms and

represents a key parameter influencing the heating efficiency of magnetic nanoparticles in alternating magnetic fields [4][6].

The heating efficiency of magnetic nanoparticles is typically characterized by the volumetric power density *P*. It depends on several factors, including the amplitude and frequency of the applied magnetic field as well as the magnetic and physical properties of the nanoparticles. Parameters such as particle size and the viscosity of the surrounding medium strongly influence the magnetic relaxation processes and therefore affect the heat generation capability of the nanoparticles [7][10]. Optimization of these parameters is essential for achieving efficient heating while maintaining safe exposure conditions for patients.

Another important factor affecting the temperature distribution during hyperthermia therapy is the geometry and volume of the heated region. The shape and size of the tumour influence heat transfer and thermal dissipation within biological tissues, which in turn affect the temperature achieved during treatment. Therefore, the concentration of magnetic nanoparticles required to obtain therapeutic temperatures may vary depending on the geometry of the treated region. Numerical modelling and computational simulations are widely used to analyse such effects and to optimize treatment parameters prior to clinical applications [5][11].

Although numerous studies have focused on the magnetic properties of nanoparticles and the influence of magnetic field parameters on heating efficiency, relatively little attention has been devoted to the influence of tumour geometry on the concentration of nanoparticles required to achieve therapeutic temperatures. Most studies assume simplified tumour geometries or focus primarily on nanoparticle properties, while the influence of the size and shape of the heated region on the required nanoparticle concentration is less frequently analysed [12][14].

The aim of this study was therefore to determine the concentration of magnetic nanoparticles required to achieve therapeutic temperatures in prostate cancer treatment using magnetic hyperthermia, taking into account the influence of the geometry and volume of the heated region. An air coil generating an alternating magnetic field was developed to obtain a uniform electromagnetic field distribution in the prostate region. Numerical simulations were performed using the Sim4Life software [21] for a prostate tumour and three simplified geometric models: a cylinder, a sphere and a cube. Heat generation by magnetic nanoparticles was calculated using the theoretical model proposed by Rosensweig [19], which enabled the estimation of the nanoparticle concentration required to achieve the therapeutic temperature.

2. Materials and Methods

2.1 Numerical Model of the Electromagnetic Field

The electromagnetic field distribution was calculated using the magneto-quasi-static formulation implemented in the simulation environment. In this approach, the electromagnetic field was described by the following equation:

$$\nabla \cdot \sigma \nabla \phi = -\mathrm{j}\omega \nabla \cdot (\sigma \mathbf{A}) \tag{1}$$

where σ is the electric conductivity, ϕ stands for the electric scalar potential, ω represents the angular frequency and **A** is the magnetic vector potential. The equation was considered together with zero Neumann boundary condition which corresponds to a vanishing normal current flux at the boundaries of the computational domain.

The simulations were performed using a real-valued solver. The electric field (*E*-field) was calculated only within the lossy ($\sigma \neq 0$) regions of the model, while the magnetic field (*H*-field) was evaluated throughout the entire computational domain. Consequently, the numerical grid was defined primarily within the lossy domain where energy dissipation occurs. The external electromagnetic excitation generated by the coil was expressed using the vector potential formulation. The *E*-field was obtained from the vector potential using tricubic interpolation, while the magnetic flux density was used to determine both the magnetic field intensity and the magnetic flux density distributions [21].

If the vector potential is not explicitly defined, it can be calculated using the Biot–Savart law:

$$\mathbf{A}(\mathbf{r}) = \frac{\mu_0}{4\pi} \int_{\Omega} \frac{\boldsymbol{J_0}(\boldsymbol{r}')}{|\mathbf{r} - \boldsymbol{r}'|} d^3\boldsymbol{r}' \tag{2}$$

where $\boldsymbol{J_0}$ is the current density vector and H-field can be expressed as:

$$H = \mu_0^{-1} \nabla \times A \tag{3}$$

This formula allows the magnetic field generated by the current-carrying coil to be determined. In this case, the low-frequency current sources must remain outside the lossy computational domain in order to avoid numerical singularities in the field calculations [21].

In magnetic hyperthermia, when magnetic nanoparticles are exposed to *H*-field, magnetic power losses are generated according to the following formula [19]:

$$P = \mu_0 \pi \chi'' f H^2 \quad (4)$$

where f is the frequency and H represents the magnetic field strength amplitude. Imaginary part of the magnetic susceptibility χ''can be calculated according to the equation [19]:

$$\chi'' = \frac{\omega \tau_{\text{eff}}}{1 + (\omega \tau_{\text{eff}})^2} \chi_0 \quad (5)$$

where $\chi_0$is the field-dependent susceptibility and ω stands for the angular frequency ($\omega = 2\pi f$). The effective relaxation time τ_{eff} may be described by the formula:

$$\frac{1}{\tau_{\text{eff}}} = \frac{1}{\tau_{\text{B}}} + \frac{1}{\tau_{\text{N}}} \quad (6)$$

where τ_{B} is the Brownian-, τ_N is the Neel- relaxation time defined as follows:

$$\tau_{\text{B}} = \frac{3\eta V_{\text{H}}}{k_{\text{B}} T} \quad (7)$$

$$\tau_N = \tau_0 e^{\frac{K V_{\text{M}}}{k_{\text{B}} T}} \quad (8)$$

and η is the viscosity, k_{B} stands for the Boltzmann constant (k_{B}=1.38·10^{-23}JK^{-1}), T is the absolute temperature. V_{H} represents the hydrodynamic volume of the particle and was given by:

$$V_{\text{H}} = \left(1 + \frac{\delta}{R_{\text{M}}}\right)^3 \cdot V_{\text{M}} \quad (9)$$

where δ represents the surfactant layer thickness, V_{M} is the magnetic volume of magnetic nanoparticles with radius R_{M}, K is the anisotropy constant of the magnetic material.

Susceptibility χ_0 used in Eq. (5) is defined as:

$$\chi_0 = \chi_{\text{i}} \frac{3}{\xi} (\coth \xi - \frac{1}{\xi}) \quad (11)$$

where χ_{i} is initial susceptibility and can be calculated from the formula:

$$\chi_{\text{i}} = \frac{\mu_0 \varphi M_{\text{d}}^2 V_{\text{M}}}{3 k_{\text{B}} T} \quad (12)$$

where φ is the concentration of magnetic nanoparticles, M_d is the domain magnetization of the suspended particles. Langevin parameter ξ used in Eq. (11) is expressed as:

$$\xi = \frac{\mu_0 M_\mathrm{d} H V_\mathrm{M}}{k_\mathrm{B} T} \tag{13}$$

2.2 Thermal simulations

The thermal simulations were based on the solution of the heat transfer equation which describes temperature evolution in biological tissues. Heat transport in the tissue was modelled using the Pennes bioheat equation, which accounts for thermal conduction, blood perfusion and metabolic heat generation [15]:

$$\rho c \frac{\partial T}{\partial t} = \nabla \cdot (k \nabla T) + Q_\mathrm{perf} + Q_\mathrm{met} + P \tag{14}$$

where T is the tissue temperature, ρ and c denote the density and specific heat of the tissue, k is the thermal conductivity. The term Q_perf represents heat exchange due to blood perfusion, Q_met is the metabolic heat generation and P represents the external heat source produced by magnetic nanoparticles (see Eq. 4).

To include a heat exchange between the skin and external environment, the Robin's boundary condition was applied as follows:

$$\kappa \frac{\partial T}{\partial \mathrm{n}} = h(T_\mathrm{ext} - T) \tag{15}$$

where κ is the thermal conductivity of skin, h is the heat transfer coefficient and T_ext is the external temperature [13].

Thermal calculations were performed using the structured-grid time-domain solver, which applies a finite-difference time-domain scheme on non-uniform grids. This approach allows efficient computation of temperature distributions while enabling local grid refinement in regions of particular interest. Electromagnetic heat sources obtained from the electromagnetic simulations were interpolated onto the thermal grid.

The voxel-based discretization enables simulations with a large number of computational cells, where each voxel can be assigned individual material parameters. This makes the method particularly suitable for modelling heterogeneous biological structures [21].

Taking into account the aforementioned mathematical models for the electromagnetic field and heat transfer, the following steps were performed. First, magnetic field H was obtained using Eq. 2, then the volumetric power density distribution was calculated using Eq. 4. In this way, the value of χ'' was determined at the considered frequency. Next, the Brownian and Néel relaxation times were calculated (see Eqs. 7 and 8) for superparamagnetic nanoparticles under the assumption that the optimization condition $\omega\tau_{eff} = 1$ is fulfilled. Based on Table 3 and Eq. 13, the Langevin parameter was determined. The value of χ_0 was then calculated using Eq. 5, and χ_i was obtained from Eq. 11. Finally, the concentrations of magnetic materials φ were determined using Eq. 12.

Additionally, the IT'IS Foundation tissue parameter database was used [2]. The tissue properties were recalculated for a frequency of f = 100 kHz, assuming that all modeled materials are uniform and not temperature dependent. In Table 1, only prostate and the tumor's dielectric properties were gathered as crucial ones for the temperature analysis.

Table 1. Thermophysical and electromagnetic properties of prostate and tumor tissue for frequency f=100 kHz used in Pennes bioheat equation and in magneto-quasi static solver [2].

Tissue name	**Mass density**	**Specific heat capacity**	**Thermal conductivity**	**HGR [W/kg]**	**HTR [W/m^3/K]**	**Conductivity**
	ρ **[kg/m^3]**	c **[J/kg/K]**	k **[W/m/K]**			σ **[S/m]**
Prostate	1045.0	3760.0	0.5115	6.10369	27820.2	$4.39 \cdot 10^{-1}$
Tumour	1090.4	3421.2	0.4500	0.9061	2705.95	$3.63 \cdot 10^{-1}$

HGR – Heat Generation Rate per unit mass;

HTR – Heat Transfer Rate coefficient per unit volume and temperature difference

2.3 Computer modelling and simulation

An air coil with a radius of 350 mm, consisting of 27 turns made of wire with a radius of 3 mm, was designed in the Sim4Life software. The turns were spaced 11 mm apart. A human model was imported from The Computable Virtual Population [24] and positioned with its arms

raised to prevent them from overheating. The position of the coil was adjusted so that the prostate gland was located at its center point as depicted in Fig. 1.

Magneto quasi-static simulations were performed assuming an alternating current with an amplitude of I_{max} = 75 A and a frequency of f = 100 kHz. For safety reasons, the parameters of the alternating magnetic field satisfied the Atkinson–Brezovich criterion i.e. $f \cdot H \leq 4.85 \cdot 10^8$ A m^{-1} s^{-1} [8]. In the present study, the selected values of the magnetic field amplitude $f \cdot H = 2.67 \cdot 10^8$ satisfy this condition, ensuring that the simulated hyperthermia treatment remains within the accepted limits for biomedical applications.

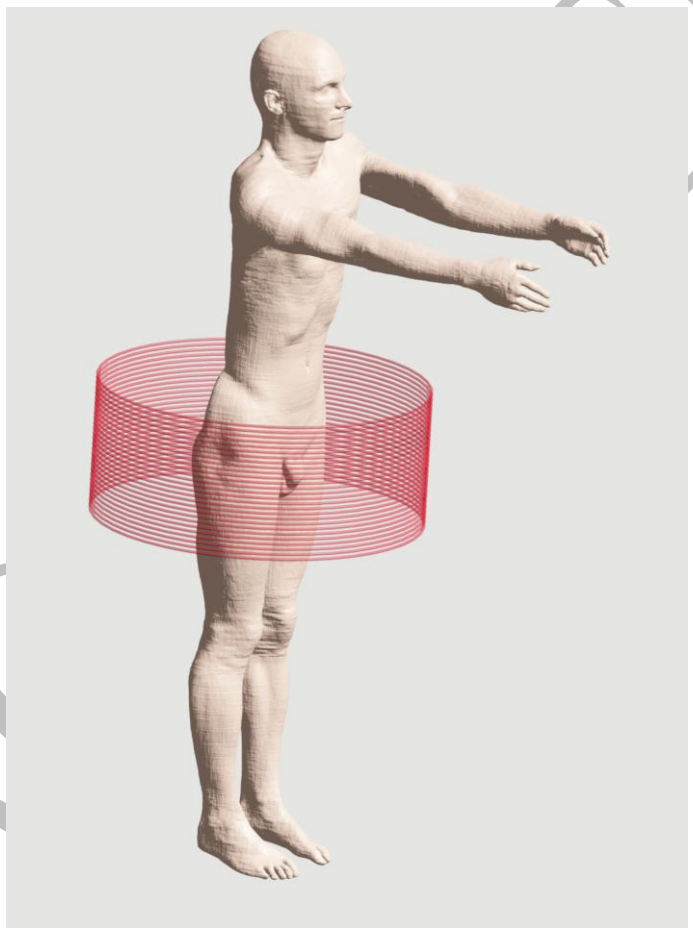

Fig.1. The designed air coil and the human model.

The naturalistic irregular tumour model was taken from freely available database [3], and three geometric primitives were analyzed: a cube with a side length a = 9 mm, a cylinder with a radius r = 4 mm and a height h = 10.5 mm, and a sphere with a radius R = 5.48 mm. The dimensions of the models were selected so that the naturalistic tumour could be inserted into them (see Fig. 2). Volume and surface area of the geometric models are gathered in Table 2.

The geometric primitives were placed in the same anatomical location within the prostate model, at the site corresponding to the location of the naturalistic tumour. At each case the electromagnetic properties of muscle tissue were assigned [14] (see Table 1).

Table 2. Volume and surface area of the analysed tumour models.

Tumour model	Dimensions [mm]	Volume [mm^3]	Area [mm^2]
Irregular	-	392.624	317.599
Cylinder	r = 4, h = 10.5	525.112	363.58
Sphere	R = 5.48	689.008	377.971
Cube	a = 9	728.489	479.669

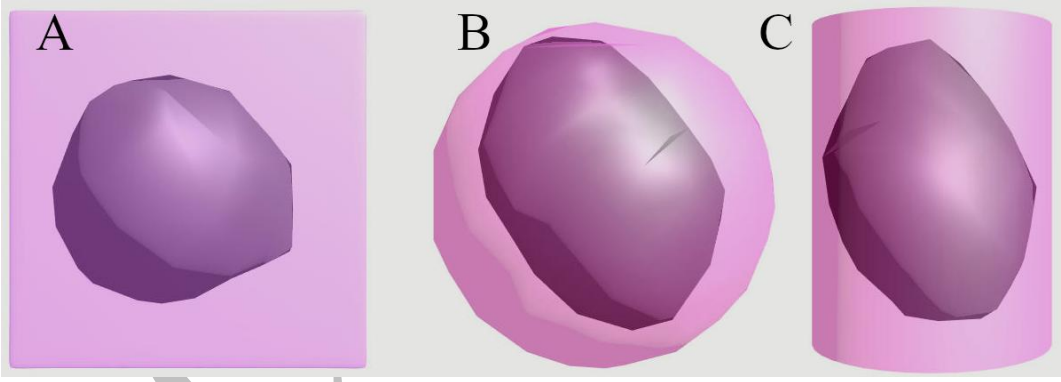

Fig.2. Comparison of geometric primitives to the naturalistic irregular tumour model: a) cube, b) sphere, c) cylinder.

~~First, magnetic field *H* was obtained using Eq. 2. Next, the input data for the thermal simulations was the volumetric power density distribution calculated using Eq. 4.~~

As for the temperature analysis, the initial human body temperature was set to 37°C and the mixed boundary conditions were applied. The heat transfer coefficient was set to h = 5 W/m^2/K, which corresponds to natural air convection [9]. In this context, the concentrations of magnetic nanoparticles φ needed to achieve the therapeutic temperature, i.e. 43 - 44°C were

evaluated. Using the relationships described by Eq. 4-13, the concentration was determined assuming monodisperse nanoparticles (see Table 3).

Table 3. Properties of magnetic nanoparticles [19].

Magnetic material	M_d [kA/m]	K [kJ/m^3]
Maghemite	414	4
Magnetite	446	41
Cobalt ferrite	425	190
Barium ferrite	380	315

3. Results

The distributions of the magnetic field H (XY and XZ cross-sections) are shown in Figures 3 and 4, where the prostate gland is marked in white at the center. It can be seen that the prostate is located in a homogeneous magnetic field region H with a value of 2.670 kA/m.

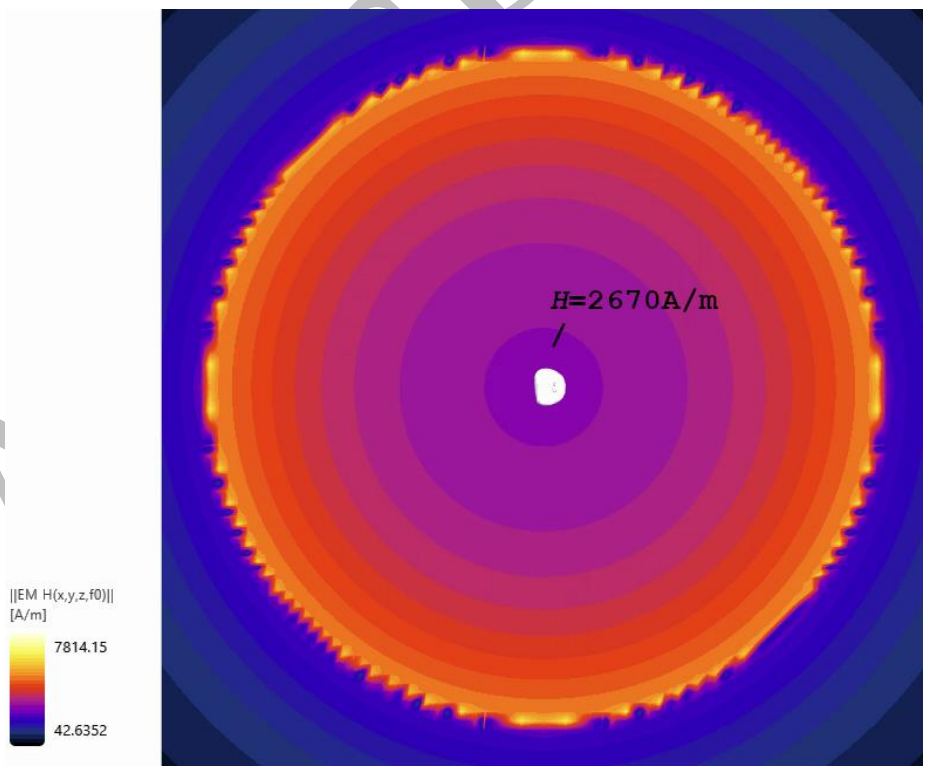

Fig.3. Magnetic field distribution (H) in the XY cross-section for f = 100 kHz with regard to the prostate (white).

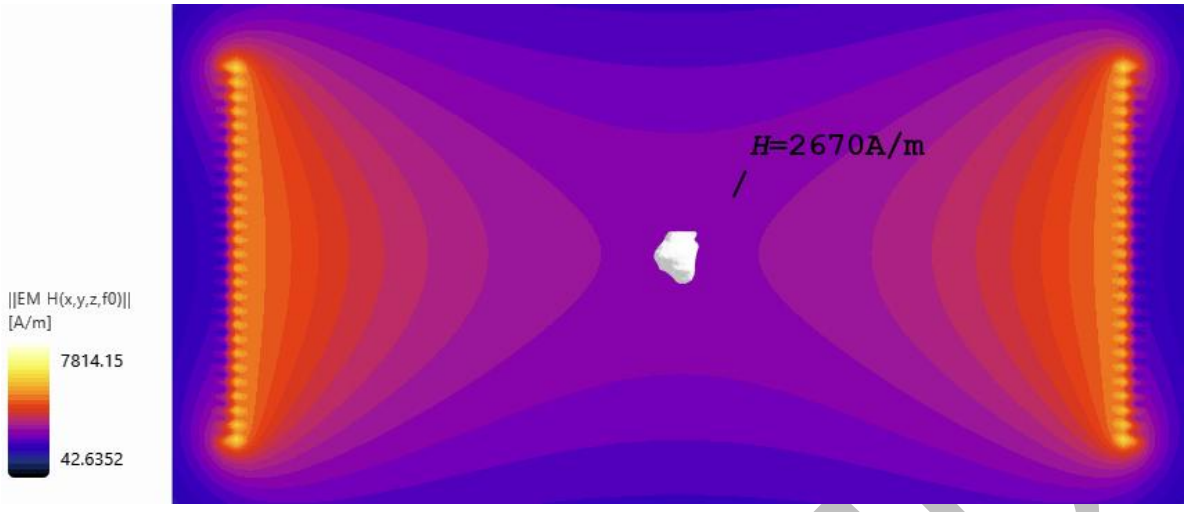

Fig.4. Magnetic field distribution (H) in the XZ cross-section for f = 100 kHz with regard to prostate (white).

In thermal simulations, the distribution of the volumetric power density P generated by magnetic nanoparticles inside the tumour models was used as the source. It was evaluated with usage of Eq.4 and the calculations were performed under the assumption that ferrofluid viscosity was η = 0.0025 kg/(m·s), surfactant layer thickness was δ = 1 nm, attempt time was τ_0 = 1 ns. Considering the optimization condition $\omega\tau_{eff}$ = 1, the magnetic radius, R_M, was estimated for magnetic nanoparticles listed in Tab. 3. It was found that R_M = 5 nm for both barium ferrite and cobalt and R_M = 13 nm for maghemite. Magnetite was excluded because the condition was not satisfied. Next, the parameters that allow achieving the therapeutic temperatures across different models regarding magnetic material were estimated (see Table 4). In the case of tumour, a power density of 712.9 kW/m^3 is required to reach the therapeutic temperature; however, depending on the magnetic material, different concentrations of magnetic nanoparticles (MNPs) must be used – for example, a concentration φ = 0.44% for maghemite, 5.5% for cobalt ferrite and 6.87% for barium ferrite.

Table 4. Comparison of magnetic nanoparticle parameters required to achieve therapeutic temperatures in different tumour models for H = 2.67 kA/m and f = 100 kHz.

Tumour model	φ (%)			Maximum power density
	Maghemite	Cobalt ferrite	Barium ferrite	P (W/m^3)
naturalistic	0.489	5.49	6.87	712890
cylinder	0.293	3.30	4.12	427734

sphere	0.269	3.02	3.78	392089
cube	0.244	2.75	3.43	356445

Figure 5 presents the distribution of power density *P* (XY- and XZ-cross-section) for the analysed tumour models. The highest values are observed for the naturalistic tumour represented by the red curve, which reaches maximum value of *P* of about 700 kW/m³ in the central region. Much lower values occur for the cylindrical model, where the power density stabilizes at around 430 kW/m³ across a similar range. The black curve, which represented spherical model shows moderate values, peaking at approximately 400 kW/m³, with a more rounded profile indicating smoother transitions. The lowest power density *P* is recorded for the cubic model, with values around 350 kW/m³ in the center. For all models, the values decrease towards the edges and approach zero.

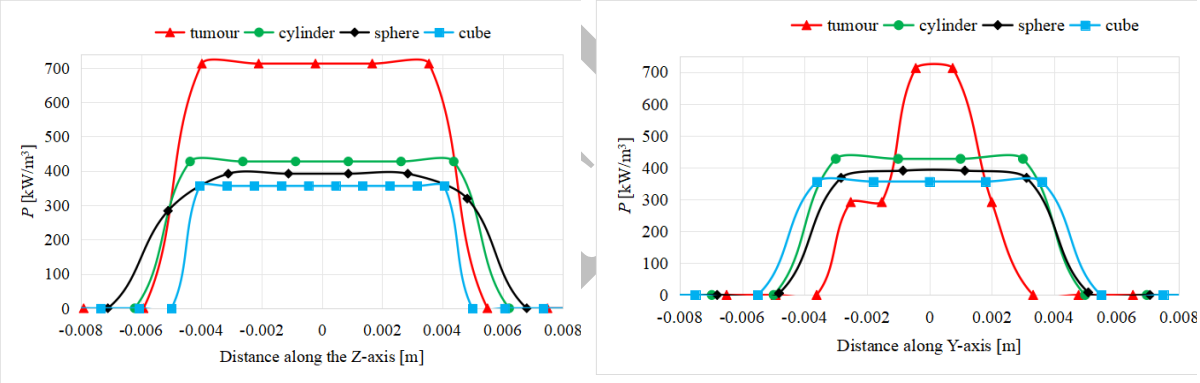

Fig.5. Volumetric power density *P* required to achieve therapeutic temperature in the analysed tumour models (XY cross-section (left) and XZ cross-section (right))

In the next step, the analysis was conducted to identify differences in the temperatures obtained for the naturalistic tumor model and the primitive models. This demonstrated how the assumed tumour's shape can influence quantitative temperature analyses. For this purpose, the power density required from MNPs to achieve the therapeutic temperature for naturalistic tumour was taken from Table 4, and the same value was then used to calculate the temperature for the geometric primitives i.e. for cylinder, sphere and cube. An analogous methodology was adopted for the other cases, i.e., the power density, which is the source of the therapeutic temperature for one of the geometric primitives, was used to estimate the temperature for the other tumour models. The temperature over time for naturalistic tumour, cylindrical, spherical

and cubic models has been collected in Fig. 6, where each of the tumour model was used as the reference to the others. Furthermore, it can be seen that the temperature stabilized after about 500 seconds in all tumor models, but the heating time was 60 minutes in all cases (the graphs have been shortened due to practical reasons). It should be noted that the main reason for the prolonged heating time and slow rise in temperature is the occurrence of necrosis.

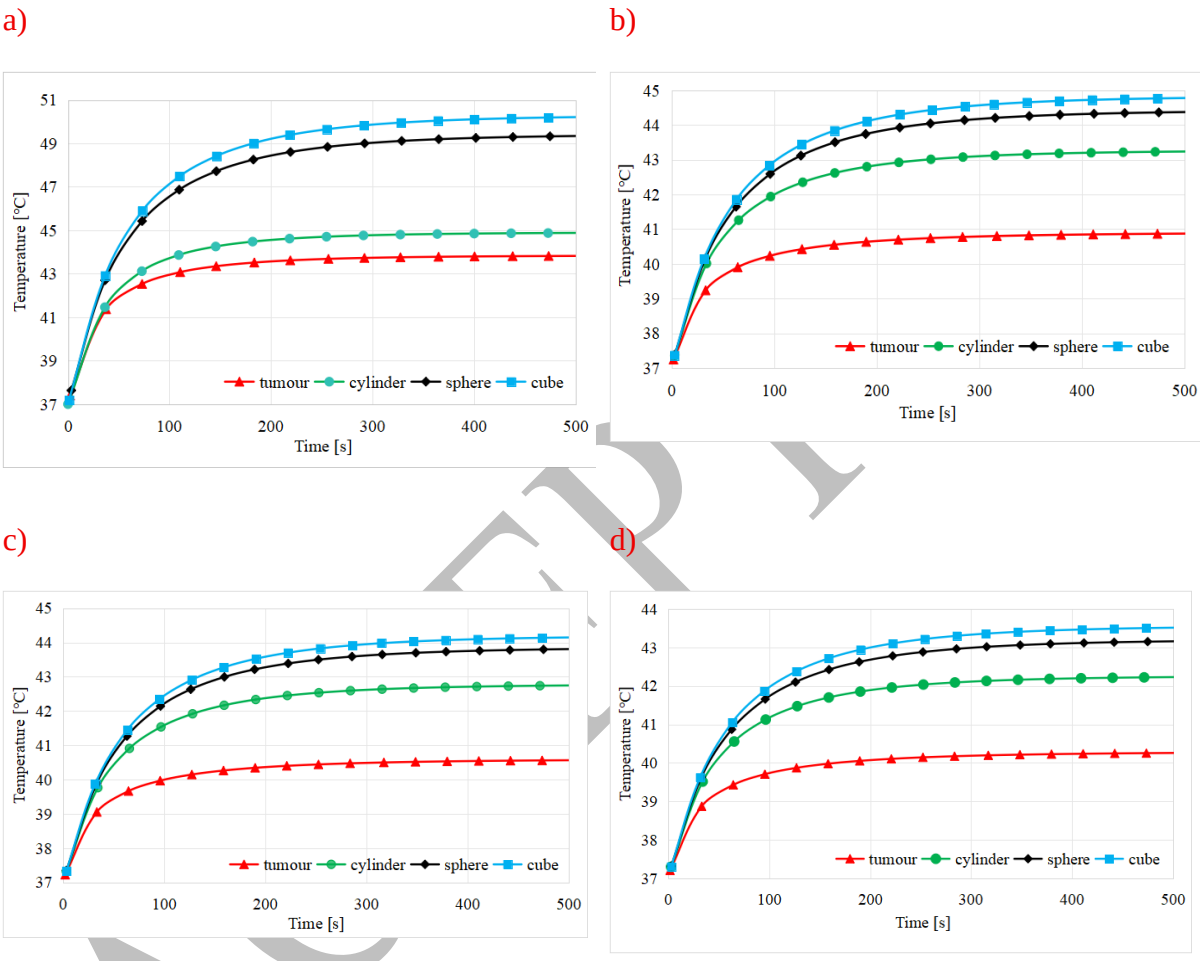

Fig.6. The temperature rise over time in analysed models regarding (a) naturalistic tumour (P=712890 W/m^3), (b) cylinder (P=427734 W/m^3), (d) sphere (P=392089 W/m3), (e) cube (P=356445 W/m3).

The concentrations of magnetic materials that allowed the required temperature to be achieved in the naturalistic tumour model were as follows: for maghemite φ = 0.489%, for cobalt ferrite φ = 5.49% and for barium ferrite φ = 6.87% (Fig.6-a). The maximum value of volumetric power density was P = 713 kW/m^3. In the case of other considered models, the temperature exceeded the acceptable range for the same power density.

The results shown in Fig.6-b were obtained for the power density was equal to P = 428 kW/m^3. In this case the cylindrical tumour model was the reference one. The concentrations of magnetic materials were as follows: for maghemite φ = 0.293%, for cobalt ferrite φ = 3.30% and for barium ferrite φ = 4.12%. It can be seen that the temperature in the naturalistic tumour model remained below the desired range. In the cylindrical model, the temperature reached the therapeutic level. In the remaining models, the temperature exceeded the required limits.

The following values of magnetic materials enabled achieving the therapeutic temperature in the spherical model (Fig. 6-c): maghemite φ = 0.269%, cobalt ferrite φ = 3.02%, and barium ferrite φ = 3.78%. The maximum value of volumetric power density was equal to P = 392 kW/m^3. In the naturalistic tumour model, the achieved temperature was much below the acceptable range. As in the case of the previous model, the temperature in the cylindrical model remained below the desired limits. In the cubic model, the temperature exceeded the required range.

Finally, the results shown in Fig.6-d were evaluated for the cubic model as the reference. The volumetric power density was P = 356 kW/m^3 and the following values of the concentrations of magnetic materials were used: for maghemite φ = 0.244%, for cobalt ferrite φ = 2.75% and for barium ferrite φ = 3.43%. In this case, the temperature increased to the therapeutic level the cubic and in the spherical models. It is worth noting that, in the other considered models, the temperature was below the acceptable range.

Discussion

The highest values of nanoparticle concentrations (φ) and the volumetric power density (P) are observed for the naturalistic tumour model. There the nanoparticle concentration reaches φ = 0.489% for maghemite, φ = 5.49% for cobalt ferrite and φ = 6.87% for barium ferrite, resulting in the highest power density P. For models such as the cylinder, sphere and cube, the concentration φ decrease, leading to a gradual reduction in generated volumetric power P. A consistent trend can be observed across all models: larger nanoparticle concentration corresponds to increased heat generation and temperature.

It can also be observed that for spherical and cubic models, the temperature difference is the smallest, ranging from 0.5°C to 1°C relative to each other. However, when comparing the spherical and cubic models with the naturalistic model, the temperature difference is the greatest. This may mean that simplifying the tumor model to a sphere or cylinder results in the greatest discrepancies.

In the case of the cylindrical model, the obtained temperatures were always between those of the naturalistic model and the spherical and cubic models. It is worth noting that in the case of this simplification, the temperature difference was smallest when the naturalistic model served as the reference one (see Fig. 6a). This may indicate that in this case, simplifying the model will result in the smallest differences in temperature estimation.

The simulations revealed that the geometry and size of the heated region significantly influence the resulting temperature distribution. When the same nanoparticle concentrations were applied to the geometric primitives, the maximum temperatures exceeded the therapeutic range. To obtain temperatures at the therapeutic level for geometric primitives, it was necessary to reduce the concentration of magnetic nanoparticles. This confirms that accurate estimation of nanoparticle concentration is essential for safe and effective hyperthermia treatment. Excessive heating could potentially damage surrounding healthy tissue.

In studies on magnetic hyperthermia, tumour regions are often simplified and represented by basic geometrical shapes such as spheres, cylinders, or cubes [1][17]. However, the results of the present simulations suggest that this approach may be inappropriate. Significant differences were observed in heat generation induced by magnetic nanoparticles between the naturalistic tumour model and simplified geometries. These discrepancies show that simplifying the geometry or geometry can lead to inaccurate predictions of temperature distribution and heating efficiency. Therefore, this approach should be used with caution when modelling magnetic hyperthermia.

It should also be noted that the simulations were performed under several simplifying assumptions, such as uniform nanoparticle distribution, monodisperse particle size and constant thermophysical properties of the tissue. In real biological conditions, factors such as polydispersion and non-uniform nanoparticle distribution may influence the temperature distribution. Therefore, further studies, including more complex models, may improve the accuracy of the predictions.

Conclusions

The study showed that the geometry and size of the heated region have a significant influence on the resulting temperature distribution. When the same nanoparticle concentrations were applied to geometric primitives such as a cylinder, sphere and cube, the obtained temperatures varied and exceeded the therapeutic range. Therefore, it was necessary to reduce the nanoparticle concentration to maintain the temperature within the desired therapeutic limits.

It indicates that the concentration of magnetic nanoparticles required for effective hyperthermia treatment depends not only on the magnetic field parameters but also on the geometry and thermal properties of the heated region. The results show that simplifying tumour geometry to basic shapes may lead to significant inaccuracies in predicting heating efficiency in magnetic hyperthermia. Accurate estimation of nanoparticle concentration is therefore essential to ensure safe and controlled temperature increase during therapy.

References

[1] Attaluri A., Kandala S.K., Zhou H., Wabler M., DeWeese T.L., Ivkov R., Magnetic nanoparticle hyperthermia for treating locally advanced unresectable and borderline resectable pancreatic cancers: the role of tumor size and eddy-current heating, Int J Hyperthermia, 2020, 37(3):108–119. DOI: 10.1080/02656736.2020.1798514.

[2] Baumgartner C., Hasgall P.A., Di Gennaro F., Neufeld E., Lloyd B., Gosselin M.C., Payne D., Klingenböck A., Kuster N., IT'IS Database for thermal and electromagnetic parameters of biological tissues, Version 5.0, August 21, 2025, DOI: 10.13099/VIP21000-05-0. itis.swiss/database. Access: 16.03.2026.

[3] Bressem K., Models for Prostate158, Version 1, Zenodo, 2022, DOI: 10.5281/zenodo.6397057. Access: 16.03.2026.

[4] Carrey J., Mehdaoui B., Respaud M., Simple models for dynamic hysteresis loop calculations of magnetic single-domain nanoparticles, J Appl Phys, 2011, 109(8), DOI:10.1063/1.3551582.

[5] Dennis C.L., Ivkov R., Physics of heat generation using magnetic nanoparticles for hyperthermia, Int J Hyperther, 2013, 29(8):715-729, DOI:10.3390/nano5010063.

[6] Dutz S., Hergt R., Magnetic nanoparticle heating and applications, Nanotechnology, 2014, 25(45), DOI: 10.1088/0957-4484/25/45/452001.

[7] Fortin J.P., Wilhelm C., Servais J., Ménager C., Bacri J.C., Gazeau F., Size-sorted anionic iron oxide nanomagnets as colloidal mediators for magnetic hyperthermia, J Am Chem Soc, 2007, 129(9):2628-2635, DOI:10.1021/ja067457e.

[8] Herrero de la Parte B., Rodrigo I., Gutiérrez-Basoa J., Iturrizaga Correcher S., Mar Medina C., Echevarría-Uraga J.J., Garcia J.A., Plazaola F., García-Alonso I., Proposal of new safety limits for in vivo experiments of magnetic hyperthermia antitumor therapy, Cancers (Basel). 2022, 14(13):3084. DOI: 10.3390/cancers14133084.

[9] Incropera F. P., DeWitt D. P., Bergman T. L., Lavine A. S., Fundamentals of Heat and Mass Transfer, John Wiley & Sons, 2011.

[10] Kafrouni L., Savadogo O., Recent progress on magnetic nanoparticles for magnetic hyperthermia, Prog Biomater, 2016, 5:147–160, DOI: 10.1007/s40204-016-0054-6.

[11] Kallumadil M., Tada M., Nakagawa T., Abe M., Southern P., Pankhurst Q.A., Suitability of commercial nanoparticles for magnetic hyperthermia, J Magn Magn Mater, 2009, 321(10):1509-1513, DOI:10.1016/j.jmmm.2009.02.075.

[12] Mahesh N., Singh N., Talukdar P., In-silico investigation of magnetic nanoparticle hyperthermia treatment to estimate the power density and concentration required to achieve the therapeutic effect, 2022, Int Commun Heat Mass Transf, 137:106295, DOI: 10.1016/j.icheatmasstransfer.2022.106295.

[13] Marusic-Paloka E., Pazanin, I., The Robin boundary condition for modelling heat transfer, 2024, Proc. R. Soc. A. 480(2286), DOI: 10.1098/rspa.2023.0850.

[14] Miaskowski A., Gas P., Numerical Estimation of SAR and Temperature Distributions inside Differently Shaped Female Breast Tumors during Radio-Frequency Ablation, 2023, Materials, 16(1):223, DOI: 10.3390/ma16010223.

[15] Pennes H. H., Analysis of tissue and arterial blood temperatures in the resting human forearm, J Appl Physiol, 1948, 1(2)93-122, DOI: 10.1152/jappl.1948.1.2.93.

[16] Pernar C. H.,The epidemiology of prostate cancer, CSH Perspect Med, 2018, 8(12), DOI: 10.1101/cshperspect.a030361.

[17] Polychronopoulos N.D., Gkountas A.A., Sarris I.E., Spyrou L.A., A computational study on magnetic nanoparticles, hyperthermia of ellipsoidal tumors, Appl Sci, 2021, 11(20):9526. DOI: 10.3390/app11209526.

[18] Rebello R.J., Oing, C., Knudsen, K.E., Prostate cancer, Nat Rev Dis Primers, 2021, 7(9), DOI: 10.1038/s41572-020-00243-0.

[19] Rosensweig R.E., Heating magnetic fluid with alternating magnetic field, J Magn Magn Mater, 2002, 252:370-374.

[20] Siegel R.L., Miller K.D., Jemal A., Cancer statistics, CA-Cancer J Clin, 2020, 70(1):7-30

[21] Sim4Life: https://sim4life.swiss/ Access: 16.03.2026.

[22] Suriyanto A., Ng, E.Y.K., Kumar S.D., Physical mechanism and modeling of heat generation and transfer in magnetic fluid hyperthermia through Néelian and Brownian relaxation: a review. BioMed Eng OnLine, 2017, 16(1), DOI: 10.1186/s12938-017-0327-x.

[23] Xiong L., Liang B., Yu K., Magnetic hyperthermia in oncology: Nanomaterials-driven combinatorial strategies for synergistic therapeutic gains, Mater Today Bio. 2025, 33, DOI: 10.1016/j.mtbio.

[24] https://itis.swiss/virtual-population/virtual-population/vip3 Access: 09.04.2026